Report

Current Biology

Purification of functional *Plasmodium falciparum* tubulin allows for the identification of parasite-specific microtubule inhibitors

Graphical abstract

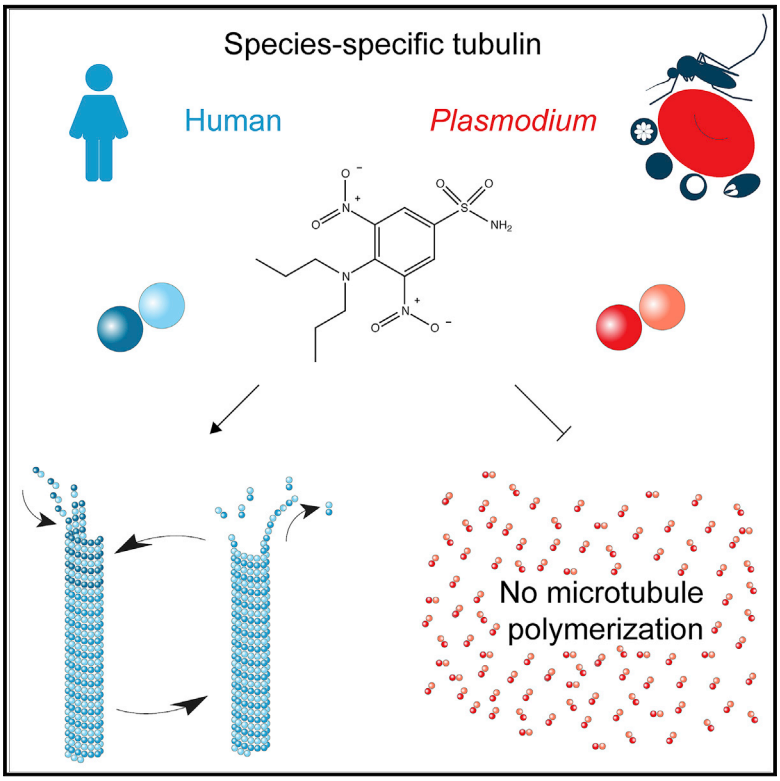

Authors

William G. Hirst, Dominik Fachet, Benno Kuropka, Christoph Weise, Kevin J. Saliba, Simone Reber

Correspondence

simone.reber@iri-lifesciences.de

In brief

Hirst et al. report the purification of tubulin from *Plasmodium*, the causative agent of malaria. Blood-stage tubulin assembles into microtubules with similar dynamic characteristics to mammalian microtubules. Two compounds show selective toxicity toward parasite tubulin and inhibit microtubule polymerization.

Highlights

- Assembly-competent tubulin was purified from *P. falciparum*-infected erythrocytes
- Blood-stage tubulin is composed of the α1β-isoforms and carries minor PTMs
- *Pf* microtubules show similar *in vitro* dynamics to mammalian microtubules
- Compounds inhibit parasite but not human microtubule growth

Hirst et al., 2022, Current Biology *32*, 919–926
February 28, 2022
https://doi.org/10.1016/j.cub.2021.12.049

CellPress

Current Biology

CellPress

Report

Purification of functional *Plasmodium falciparum* tubulin allows for the identification of parasite-specific microtubule inhibitors

William G. Hirst,[1,2] Dominik Fachet,[1,2] Benno Kuropka,[3] Christoph Weise,[3] Kevin J. Saliba,[2] and Simone Reber[1,4,5,6,*]
[1]IRI Life Sciences, Humboldt-Universität zu Berlin, 10115 Berlin, Germany
[2]Research School of Biology, The Australian National University, Canberra, ACT 2601, Australia
[3]Freie Universität Berlin, Institute of Chemistry and Biochemistry, Core Facility BioSupraMol, 14195 Berlin, Germany
[4]University of Applied Sciences Berlin, 13353 Berlin, Germany
[5]Twitter: @SimoneReber
[6]Lead contact
*Correspondence: simone.reber@iri-lifesciences.de
https://doi.org/10.1016/j.cub.2021.12.049

SUMMARY

Cytoskeletal proteins are essential for parasite proliferation, growth, and transmission, and therefore have the potential to serve as drug targets.[1–5] While microtubules and their molecular building block αβ-tubulin are established drug targets in a variety of cancers,[6,7] we still lack sufficient knowledge of the biochemistry of parasite tubulins to exploit the structural divergence between parasite and human tubulins. For example, it remains to be determined whether compounds of interest can specifically target parasite microtubules without affecting the host cell cytoskeleton. Such mechanistic insights have been limited by the lack of functional parasite tubulin. In this study, we report the purification and characterization of tubulin from *Plasmodium falciparum*, the causative agent of malaria. We show that the highly purified tubulin is fully functional, as it efficiently assembles into microtubules with specific parameters of dynamic instability. There is a high degree of amino-acid conservation between human and *P. falciparum* α- and β-tubulin, sharing approximately 83.7% and 88.5% identity, respectively. However, *Plasmodium* tubulin is more similar to plant than to mammalian tubulin, raising the possibility of identifying compounds that would selectively disrupt parasite microtubules without affecting the host cell cytoskeleton. As a proof of principle, we describe two compounds that exhibit selective toxicity toward parasite tubulin. Thus, the ability to specifically disrupt protozoan microtubule growth without affecting human microtubules provides an exciting opportunity for the development of novel antimalarials.

RESULTS AND DISCUSSION

Purification of assembly-competent tubulin from *P. falciparum*-infected erythrocyte cultures

As the asexual blood stages of *P. falciparum* are responsible for the clinical symptoms of malaria and can be readily cultured in the lab,[8,9] we decided to purify tubulin from infected red blood cells (Figure 1A). By sequentially lysing first the red blood cells and, in a second step, the parasites, we were able to separate the cytoplasmic content of the host cell from that of the parasites (Figure S1A). In the following step, αβ-tubulin was purified by affinity chromatography[10,11] from the parasite lysate (Figure 1B). As some previous reports suggested that human erythrocytes contain tubulin,[12,13] we monitored the presence of tubulin throughout the sequential host and parasite cell lysis (Figures 1C and S1B), and concluded that host tubulin is absent from isolated parasite lysates and from purified tubulin (see also Figure 2A). The protocol we applied captured the full complement of *P. falciparum* tubulin, indicated by a complete depletion of tubulin from the lysate (Figure 1C, F, flowthrough), confirming that we did not enrich for a tubulin subpopulation (e.g., a specific isoform or post-translational modification [PTM]). This suggests that the purified tubulin represents the physiological tubulin proteome of the *Plasmodium* blood stages (mostly late trophozoites and schizonts). Importantly, and in contrast to previous attempts,[14–16] our purified *P. falciparum* tubulin is assembly-competent and shows characteristic microtubule dynamic instability, as visualized by total internal reflection fluorescence (TIRF) microscopy (Figures 1D and E; Video S1). To our knowledge, this is the first time that active, assembly-competent tubulin has been purified from *P. falciparum*.

Blood-stage *P. falciparum* tubulin is composed of the α1- and β-isoforms

Purified tubulin populations are usually a complex mixture of isoforms with various PTMs specific for a given cell line or species.[17–19] The *P. falciparum* genome, however, only encodes for two α-tubulins and one β-tubulin (Figure S2A). To characterize the isoform composition of the purified *P. falciparum* tubulin, we measured the accurate mass of the tubulin isoforms via

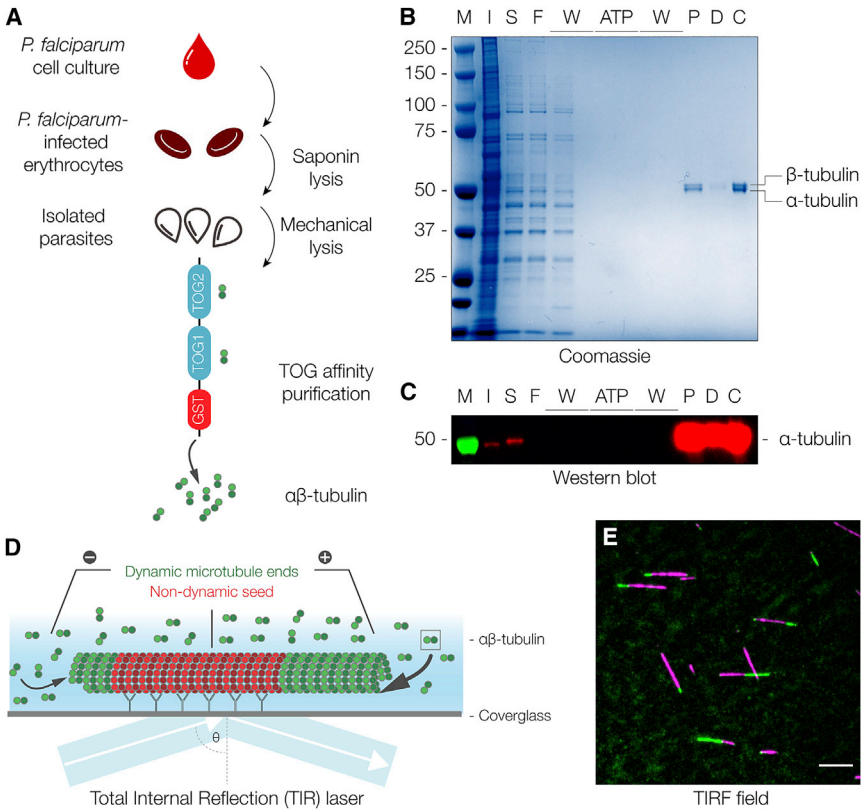

Figure 1. Affinity purification of blood-stage *P. falciparum* tubulin

(A) Strategy detailing the purification of *P. falciparum* tubulin.

(B) Coomassie-stained SDS-PAGE of the individual purification steps from *Pf* lysate. M, marker; I, input; S, supernatant; F, flowthrough; W, wash; ATP, ATP wash; P, peak fraction; D, desalt; C, concentrated.

(C) Western blot analysis with anti-α-tubulin antibody of samples shown in (B).

(D) Schematic of a microtubule assembly assay visualized by total internal reflection fluorescence (TIRF) microscopy using GMPCPP-stabilized microtubule seeds (red) as nucleation templates for dynamic microtubules (green).

(E) Representative TIRF microscopy image of dynamic *Pf* microtubules (green) grown from stabilized seeds (magenta) at 37°C and 6 μM tubulin. Scale bar: 5 μm.

See also Figure S1; Video S1.

intact protein mass spectrometry (LC-ESI-MS). The deconvoluted mass spectrum showed two main peaks (Figures 2A and S2B). The peak at 50,296 Da matches the mass predicted for α1-tubulin (Uniprot ID Q6ZLZ9, 50,297 Da) and the second major peak at 49,750 Da corresponds to β-tubulin (Uniprot ID Q7KQL5, 49,751 Da). A peak that corresponds to α2-tubulin at 49,691 Da (Uniprot ID Q8IFP3) is absent from the spectrum. However, intact protein mass spectrometry does not detect low-abundance components. To detect even minor components, we separated the purified tubulin via SDS-PAGE (Figure S2C) and identified the bands by matrix-assisted laser desorption/ionization mass spectrometry (MALDI-MS). The corresponding peptide mass fingerprints revealed the presence of *P. falciparum* α1- and β-tubulin, but not the α2-isoform (Figures S2A and S2D). This is consistent with expression data and antibody-based experiments that suggest α1-tubulin to be the predominant isoform during blood stages.[20–24] To assess the composition of the purified tubulin with greater sensitivity, we performed a trypsin in-solution digest of the purified *Plasmodium* tubulin, analyzed the resulting peptides by LC-MS/MS, and estimated the relative protein abundance using the iBAQ value.[25] Again, as main components, we identified *P. falciparum* α1- and ß-tubulin (>97% of total protein, Table S1) confirming our previous results. In addition, we detected a low-intensity background of around 50 *Plasmodium* proteins (with α2-tubulin <1% of total protein, Table S1) and human hemoglobin. This further confirmed that the purified *P. falciparum* tubulin was free of human host tubulin and free of potentially contaminating microtubule-associated proteins (MAPs) and motors.

In addition to genetic diversity, tubulins are functionalized with diverse PTMs, such as acetylation, polyglutamylation, phosphorylation, and (de-) tyrosination (as reviewed in Roll-Mecak[26] and Janke and Magiera[27]). In contrast to bovine tubulin, which is known to be heavily post-translationally modified, the purified *Plasmodium* tubulin carries almost no PTMs (Figure 2B). In line with previous reports,[24,28] we find *Plasmodium* tubulin to be tyrosinated but not acetylated. While acetylation of α-tubulin was shown to mechanically stabilize microtubules and prevent microtubule breakage,[29] it remains to be shown whether tyrosination directly renders microtubules more flexible, or indirectly via the recruitment of MAPs and motors.[30–33] Recent studies using expansion microscopy on *P. falciparum* schizonts have shown that hemispindles are not polyglutamylated, whereas the subpellicular microtubules are polyglutamylated.[34] Our intact protein mass spectrometry analysis identified a subpopulation of the purified tubulin to be monoglutamylated (Figure 2A, peak at 49,879 Da, which is likely explained by the addition of a single glutamyl modification (Δ_m = +129 Da) on β-tubulin), giving a potential explanation for why the purified tubulin is not recognized by our antibody against polyglutamylation, which requires the addition of at least two glutamyl units (Figure 2B, Poly-Glu). Polyglutamylation controls microtubule dynamics indirectly by regulating MAPs, which either leads to the enzymatic severing of microtubules[35,36] or to microtubule stabilization.[37] Thus, polyglutamylation is likely to enable both stabilization and destabilization of microtubules, depending on the cellular context. To make sure that we did not lose significant amounts of (stabilized) microtubules during the purification, we compared tubulin amounts and the PTM pattern in whole parasites, the parasite lysate, and increasing amounts of high-spin pellets. We did not find tubulin in the pellet (Figure S2E), nor did the PTM pattern change (Figure S2F). Taken together, the results from three mass spectrometry approaches and western blot analysis show that α1-tubulin is the predominant α-tubulin isoform of

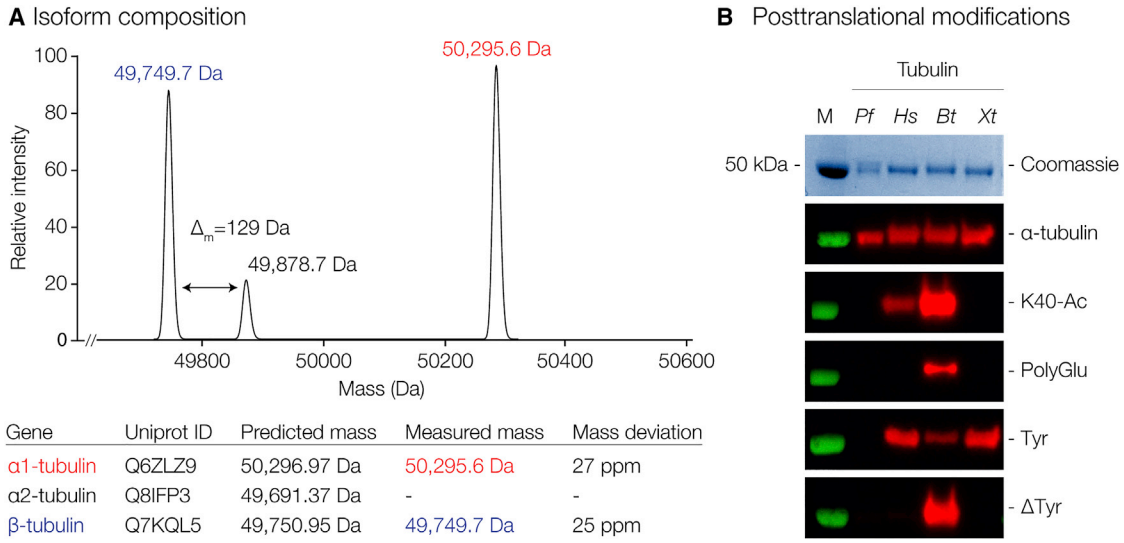

Gene	Uniprot ID	Predicted mass	Measured mass	Mass deviation
α1-tubulin	Q6ZLZ9	50,296.97 Da	50,295.6 Da	27 ppm
α2-tubulin	Q8IFP3	49,691.37 Da	-	-
β-tubulin	Q7KQL5	49,750.95 Da	49,749.7 Da	25 ppm

Figure 2. Isoform composition and post-translational modifications of purified blood-stage *P. falciparum* tubulin

(A) Deconvoluted mass spectrum of purified *Pf* tubulin. Individual tubulin isoforms are labeled in the spectrum and measured masses are compared with predicted masses in the table below. The raw mass spectrum used for deconvolution is shown in Figure S2B.

(B) Western blots probing post-translational modifications found in purified *P. falciparum* (*Pf*), HEK cells (*Hs*), bovine brain (*Bt*), and *Xenopus laevis* (*Xl*) tubulin. α-Tubulin is a loading control, K40-Ac recognizes acetylated lysine at position 40 of α-tubulin, Poly-Glu recognizes epitopes containing acidic residues modified with a chain of at least two glutamyl residues, Tyr recognizes the C-terminal EEY epitope of tyrosinated tubulin, ΔTyr recognizes the detyrosinated C-terminus of α-tubulin.

See also Figure S2; Table S1.

purified blood-stage *P. falciparum*, together with β-tubulin, with only minor PTMs.

Microtubules assembled from purified *P. falciparum* tubulin have similar dynamic characteristics to mammalian microtubules

In the *P. falciparum* blood stages, microtubules are found as both stable subpellicular microtubules and dynamic spindle microtubules.[15,38] The dynamic nature of microtubules can be empirically described by four parameters: (1) the polymerization velocity at which microtubules grow (v_g), (2) the depolymerization velocity at which microtubules shrink (v_s), (3) the catastrophe frequency at which microtubules switch from growth to shrinkage (F_{cat}), and (4) the rescue frequency at which microtubules switch from shrinkage to growth (F_{res}).[39] This dynamic behavior is intrinsic to microtubules and has not been reported for reconstituted *P. falciparum* microtubules. Using an *in vitro* reconstitution assay, together with TIRF microscopy, we assessed the dynamic parameters of purified *P. falciparum* tubulin in comparison with tubulin purified from bovine brain. Dynamic microtubule assays showed that *P. falciparum* nucleated from GMPCPP-templates at tubulin concentrations as low as 6 μM (Figure 1E), while the nucleation threshold for brain tubulin is at around 9 μM.[40] Therefore, we compared microtubule dynamics at 9 μM tubulin and 37°C (Figure 3A). Using kymograph analysis to quantify parameters of dynamic instability (Figure 3B), we found *P. falciparum* microtubules to have a polymerization velocity of 0.44 ± 0.01 μm/min (mean ± SEM), which is comparable to bovine microtubules (0.42 ± 0.01 μm/min, Figure 3C, n = 106 and 318, respectively, $p < 0.05$). *Plasmodium* microtubules depolymerize faster than bovine microtubules (13.35 ± 0.66 μm/min versus 7.78 ± 0.27 μm/min, Figure 3D, n = 96 and 174, respectively, $p < 0.0001$). The catastrophe frequency (Figure 3E), reported as the inverse of microtubule lifetime, was 0.0055 ± 0.0003 s^{-1} versus 0.0076 ± 0.0003 s^{-1} (n = 106 and 318, respectively, $p < 0.0001$) and the rescue frequency 0.0058 ± 0.0022 s^{-1} versus 0.0472 ± 0.0048 s^{-1} (Figure 3F, n = 96 and 174, respectively, $p < 0.0001$). The p value depends on the size of the data set[41] and does not necessarily tell us whether the observed differences in microtubule dynamics are physiologically relevant. We therefore compared the range of dynamic parameters of three independent *Plasmodium* tubulin purifications. The measured polymerization velocity for bovine brain microtubules (0.42 ± 0.01 μm/min) lies within the range of the mean polymerization velocities of the three independent *Plasmodium* tubulin data sets (0.31 ± 0.01 to 0.49 ± 0.01 μm/min, Figure S3). This led us to conclude that *P. falciparum* microtubules display parameters of dynamic instability similar to those of mammalian microtubules.

Microtubule-targeting compounds selectively inhibit *P. falciparum* but not human microtubule growth

To characterize parasite-specific microtubule inhibitors that do not affect host microtubules, we first aimed to identify a human tubulin population derived from actively dividing cells with dynamic properties comparable to those of *P. falciparum* microtubules, the rationale being that microtubules with similar dynamics would allow for robust interpretation of perturbation experiments. Indeed, tubulin purified from the human kidney cell line HEK293 (Figure S4A) nucleated from GMPCPP-templates at tubulin concentrations as low as 6 μM (Figure 4A), and showed similar microtubule dynamics when compared

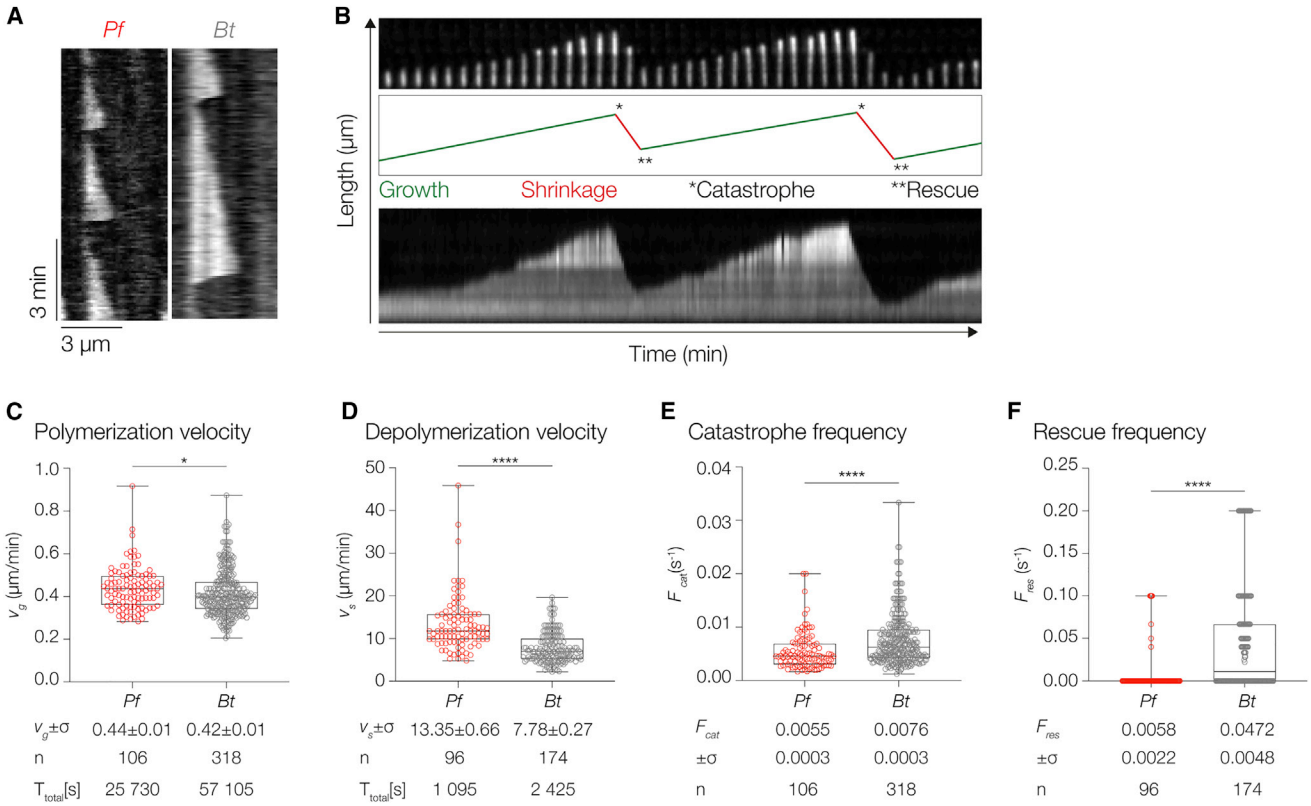

Figure 3. *P. falciparum* microtubules exhibit dynamic properties similar to mammalian microtubules *in vitro*

(A) Representative TIRF kymographs of dynamic *P. falciparum* and bovine microtubules at 37°C and 9 μM tubulin.

(B) Montage of one dynamic microtubule at different time points. Phases of dynamic instability are labeled as growth (green), shrinkage (red); transitions between growth and shrinkage are marked by * (catastrophe), transitions between shrinkage and growth by ** (rescue).

(C–F) Parameters of dynamic instability measured at 37°C and 9 μM tubulin. All values were obtained from measurements of microtubules pooled over at least three independent experiments and all p values are calculated with the Mann-Whitney test. For the modified box-and-whiskers plots, the boxes range from 25th to 75th percentile, the whiskers span the range, and the horizontal line marks the median value.

(C) *Pf* microtubules grow at 0.44 ± 0.01 μm/min (mean ± SEM), *Bt* microtubules at 0.42 ± 0.01 μm/min, with p (*Pf*, *Bt*) <0.05.

(D) *Pf* microtubules depolymerize at 13.35 ± 0.66 μm/min, *Bt* microtubules at 7.78 ± 0.27 μm/min, with p (*Pf*, *Bt*) <0.0001.

(E) Catastrophe frequencies are reported as the inverse of microtubule lifetimes. *Pf* microtubules catastrophe at 0.0055 ± 0.0003 s^{-1}, *Bt* microtubules at 0.0076 ± 0.0003 s^{-1}, with p (*Pf*, *Bt*) <0.0001.

(F) Rescue frequencies are reported as the inverse of the duration of each depolymerization event. Events without a rescue are given a value of zero. *Pf* microtubules rescue at 0.0058 ± 0.0022 s^{-1}, *Bt* microtubules at 0.0472 ± 0.0048 s^{-1}, with p (*Pf*, *Bt*) <0.0001. Total time (T_{total}) of observed microtubule growth and shrinkage and number of events (n) indicated.

See also Figure S3.

with *P. falciparum* microtubules (Figure 4B–4E). We thus concluded that human tubulin purified from actively dividing HEK293 cells was a suitable benchmark for the identification and characterization of parasite-specific microtubule inhibitors *in vitro*. Previous studies have proposed that inhibition of blood-stage *P. falciparum* cell growth by the herbicides oryzalin and amiprofos methyl (APM) is the result of the inhibition of microtubule assembly, and that these compounds selectively inhibit parasite rather than host microtubules.[14,15,42] Indeed, a dinitroaniline similar to oryzalin (Trifluralin) has been shown to have an increased affinity for parasite tubulin, and selectively inhibits parasite growth in cell culture in comparison with mammalian cells.[15] These studies, however, did not show a direct selective effect of the compounds on human versus *P. falciparum* microtubules. Therefore, we still lack mechanistic evidence that oryzalin and APM interfere with parasite microtubule dynamics and, more importantly, that microtubule inhibition is parasite-specific. To test whether inhibition of microtubule growth is indeed the molecular mechanism of action, and whether the compounds selectively interact with parasite over host microtubules, dynamic *P. falciparum* and human microtubules were assembled *in vitro* in the presence, or absence, of oryzalin or APM (Figure 4F). Titrations of oryzalin showed that *P. falciparum* microtubule growth velocity decreased with increasing oryzalin, starting at 0.5 up to 5 μM with an IC_{50} of 2.4 μM, and growth was completely inhibited at 6 μM oryzalin (Figure 4G). APM also fully inhibited *P. falciparum* microtubule growth at 10 μM (Figure 4F). Importantly, both conditions did not inhibit mammalian microtubule growth, as HEK293 microtubule polymerization remained unchanged at oryzalin concentrations of up to at least 25 μM (IC_{50} = 57.5 μM) (Figure 4H), and an APM concentration of 10 μM (Figure 4F). To compare the *in vitro*

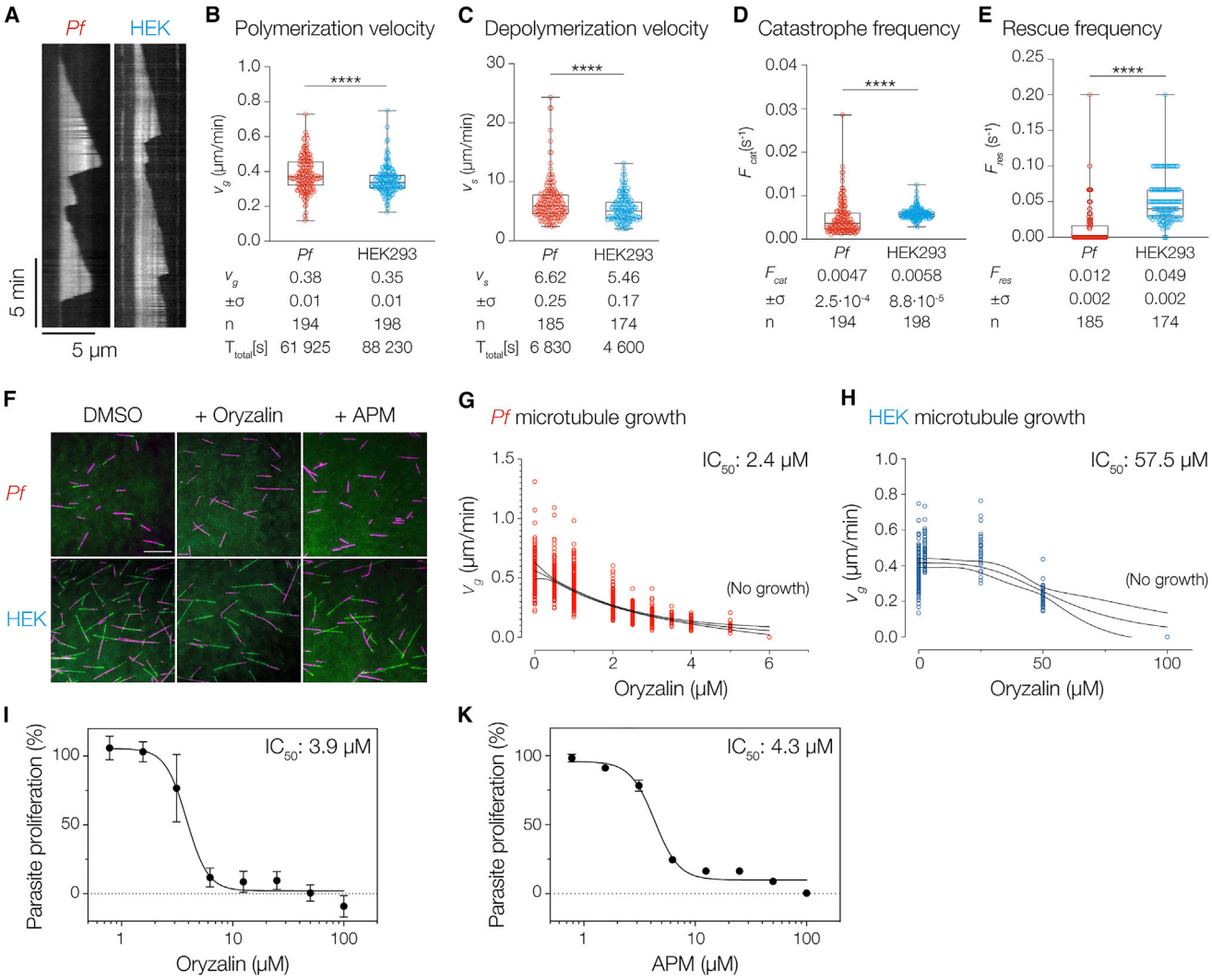

Figure 4. Oryzalin and APM are *P. falciparum*-specific microtubule inhibitors

(A) Representative TIRF kymographs of dynamic *P. falciparum* and HEK293 microtubules at 6 µM tubulin.

(B–E) Parameters of dynamic instability measured at 37°C and 6 µM tubulin. All values were obtained from measurements of microtubules pooled over at least three independent experiments, and all p values are calculated with the Mann-Whitney test. For the modified box-and-whiskers plots the boxes range from 25th to 75th percentile, the whiskers span the range, and the horizontal line marks the median value.

(B) *Pf* microtubules grow at 0.38 ± 0.01 µm/min (mean ± SEM), human microtubules at 0.35 ± 0.01 µm/min, with p (*Pf, Hs*) <0.0001.

(C) *Pf* microtubules depolymerize at 6.62 ± 0.25 µm/min, human microtubules at 5.46 ± 0.17 µm/min, with p (*Pf, Hs*) <0.0001.

(D) Catastrophe frequencies are reported as the inverse of microtubule lifetimes. *Pf* microtubules catastrophe at 0.0047 ± 2.5 × 10^{-4} s^{-1}, human microtubules at 0.0058 ± 8.8 × 10^{-5} s^{-1}, with p (*Pf, Hs*) <0.0001.

(E) Rescue frequencies are reported as the inverse of the duration of each depolymerization event. Events without a rescue are given a value of zero. *Pf* microtubules rescue at 0.012 ± 0.002 s^{-1}, human microtubules at 0.049 ± 0.002 s^{-1}, with p (*Pf, Hs*) <0.0001. Total time (T_{total}) of observed microtubule growth and shrinkage and number of events (n) indicated.

(F) Representative TIRF microscopy images of dynamic *Pf* and human HEK29 microtubules (green) grown from stabilized seeds (magenta) at 37°C and 6 µM tubulin in 1% DMSO, 2.5 µM oryzalin, or 10 µM APM. All images were captured after 10 min at 37°C. Scale bar: 10 µm.

(G) *Pf* and (H) human HEK293 microtubule growth rates in the presence of increasing oryzalin concentrations with 6 µM tubulin. For *Pf* microtubules, 459, 251, 397, 502, 261, 119, 42, 90, and 30 growth events were measured at 0, 0.5, 1, 2, 2.5, 3, 3.5, 4, and 5 µM oryzalin, respectively. No growth events were observed at or above 6 µM oryzalin. For HEK 293 microtubules, 223, 57, 33, and 62 growth events were measured at 0, 2.5, 25, and 50 µM oryzalin, respectively. No growth events were observed at 100 µM oryzalin. To determine IC_{50} values, the data were fit to a four-parameter logistic regression model. Representative dose-response curves of static *Pf* cultures grown in the presence of oryzalin (I) and APM (K). Each point represents parasite proliferation relative to an untreated (100%) and chloroquine-treated (0%) control. Error bars indicate SD between replicates, and where not visible, are smaller than the symbol. Oryzalin titration data represent nine data points averaged from three independent experiments; APM titration data represent data averaged from three technical replicates. To determine IC_{50} values, the data were fit to a four-parameter logistic regression model.

See also Figure S4.

inhibition with the inhibition of blood-stage parasite growth, *P. falciparum* cultures were grown for 96 h with serial dilutions of the two compounds. Average IC_{50} values for oryzalin and APM were 3.9 ± 0.4 μM (Figure 4I) and 4.3 ± 0.5 μM (Figure 4K), respectively, which are close to previously published values.[15] Although it is difficult to compare purified protein assays (e.g., Figure 4G) to cell proliferation assays (e.g., Figure 4I), it is worth noting that similar oryzalin concentrations were required to inhibit both microtubule growth and parasite proliferation. Taken together, we have demonstrated that tubulin and microtubules purified from *P. falciparum* can be studied directly with immediate physiological relevance: oryzalin and APM both selectively inhibit *P. falciparum* over mammalian microtubule growth *in vitro*. Given the proven pharmacological value of disrupting microtubule function,[6,7] the availability of purified parasite tubulin together with the assays established here will allow for more systematic, mechanistic, and quantitative bottom-up screens for pathogen-specific microtubule inhibitors in the future.[43–46]

STAR★METHODS

Detailed methods are provided in the online version of this paper and include the following:

- KEY RESOURCES TABLE
- RESOURCE AVAILABILITY
  - Lead contact
  - Materials availability
  - Data and code availabilty
- EXPERIMENTAL MODEL AND SUBJECT DETAILS
  - Chloroquine (CQ)-sensitive 3D7 wild-type strain of *P. falciparum*
  - HEK293 cell line
- METHOD DETAILS
  - Preparation of GMPCPP-stabilized microtubule seeds
  - TIRF assays, image acquisition, and data processing
  - Synchronization of *P. falciparum* cultures
  - Purification of *P. falciparum* tubulin
  - Purification of HEK tubulin
  - Purification of bovine brain tubulin
  - Parasite proliferation assays
  - Intact protein mass spectrometry
  - Peptide mass fingerprint analysis by MALDI-MS
  - In-solution digestion of *P. falciparum* tubulin and LC-MS/MS analysis
- QUANTIFICATION AND STATISTICAL ANALYSIS

SUPPLEMENTAL INFORMATION

Supplemental information can be found online at https://doi.org/10.1016/j.cub.2021.12.049.

ACKNOWLEDGMENTS

The authors thank all past and current members of the Reber lab, in particular Sebastian Reusch and Soma Zsoter for purifying HEK293 tubulin. We thank the AMBIO (Charité, Berlin) for imaging support. For mass spectrometry, we would like to acknowledge the assistance of the Core Facility BioSupraMol supported by the Deutsche Forschungsgemeinschaft (DFG). We are grateful to Jake's Baum laboratory for providing a large-scale iRBC sample and invaluable advice on *Plasmodium* biochemistry. We thank the Matuschewski and Frischknecht laboratories for helpful discussions, and Ylva Veith for maintaining *P. falciparum* cultures. We thank the Canberra branch of the Australian Red Cross Lifeblood and the DRK Berlin for the provision of red blood cells. We thank Stefan Florian for critical comments on the manuscript. This work was supported by the Alliance Berlin Canberra "Crossing Boundaries: Molecular Interactions in Malaria," co-funded by a grant from the Deutsche Forschungsgemeinschaft (DFG) for the International Research Training Group (IRTG) 2290 and the Australian National University.

AUTHOR CONTRIBUTIONS

W.G.H. and S.R. conceived the project. W.G.H. performed all experiments and analyzed the data if not stated otherwise. D.F. contributed purified tubulin, western blot controls, and the tubulin alignments. B.K. and C.W. performed and interpreted the mass-spectrometric analyses. K.J.S. supervised the experiments with *P. falciparum* cultures. S.R. wrote the manuscript with input from all authors.

DECLARATION OF INTERESTS

The authors declare no competing interests.

Received: May 27, 2021
Revised: November 8, 2021
Accepted: December 17, 2021
Published: January 19, 2022

REFERENCES

1. Kappes, B., and Rohrbach, P. (2007). Microtubule inhibitors as a potential treatment for malaria. Future Microbiol *2*, 409–423.
2. Fennell, B.J., Naughton, J., Barlow, J., Brennan, G., Fairweather, I., Hoey, E., McFerran, N., Trudgett, A., and Bell, A. (2008). Microtubules as antiparasitic drug targets. Expert Opin. Drug Discov. *3*, 501–518.
3. Harding, C.R., and Frischknecht, F. (2020). The riveting cellular structures of apicomplexan parasites. Trends Parasitol *36*, 979–991.
4. Gaillard, N., Sharma, A., Abbaali, I., Liu, T., Shilliday, F., Cook, A.D., Ehrhard, V., Bangera, M., Roberts, A.J., Moores, C.A., et al. (2021). Inhibiting parasite proliferation using a rationally designed anti-tubulin agent. EMBO Mol. Med. *13*, e13818.
5. Schrével, J., Sinou, V., Grellier, P., Frappier, F., Guénard, D., and Potier, P. (1994). Interactions between docetaxel (Taxotere) and *Plasmodium falciparum*-infected erythrocytes. Proc. Natl. Acad. Sci. USA *91*, 8472–8476.
6. Florian, S., and Mitchison, T.J. (2016). Anti-microtubule drugs. Methods Mol. Biol. *1413*, 403–421.
7. Steinmetz, M.O., and Prota, A.E. (2018). Microtubule-targeting agents: strategies to hijack the cytoskeleton. Trends Cell Biol *28*, 776–792.
8. Trager, W., and Jensen, J.B. (1976). Human malaria parasites in continuous culture. Science *193*, 673–675.
9. Maier, A.G., Matuschewski, K., Zhang, M., and Rug, M. (2019). *Plasmodium falciparum*. Trends Parasitol *35*, 481–482.
10. Reusch, S., Biswas, A., Hirst, W.G., and Reber, S. (2020). Affinity purification of label-free tubulins from *Xenopus* egg extracts. STAR Protoc *1*, 100151. https://doi.org/10.1016/j.xpro.2020.100151.
11. Widlund, P.O., Podolski, M., Reber, S., Alper, J., Storch, M., Hyman, A.A., Howard, J., and Drechsel, D.N. (2012). One-step purification of assembly-competent tubulin from diverse eukaryotic sources. Mol. Biol. Cell *23*, 4393–4401.
12. Bryk, A.H., and Wiśniewski, J.R. (2017). Quantitative analysis of human red blood cell proteome. J. Proteome Res. *16*, 2752–2761.
13. Nigra, A.D., Casale, C.H., and Santander, V.S. (2020). Human erythrocytes: cytoskeleton and its origin. Cell. Mol. Life Sci. *77*, 1681–1694.
14. Dempsey, E., Prudêncio, M., Fennell, B.J., Gomes-Santos, C.S., Barlow, J.W., and Bell, A. (2013). Antimitotic herbicides bind to an unidentified

site on malarial parasite tubulin and block development of liver-stage Plasmodium parasites. Mol. Biochem. Parasitol. *188*, 116–127.

15. Fennell, B.J., Naughton, J.A., Dempsey, E., and Bell, A. (2006). Cellular and molecular actions of dinitroaniline and phosphorothioamidate herbicides on *Plasmodium falciparum*: tubulin as a specific antimalarial target. Mol. Biochem. Parasitol. *145*, 226–238.
16. Chakrabarti, M., Joshi, N., Kumari, G., Singh, P., Shoaib, R., Munjal, A., et al. (2021). Interaction of *Plasmodium falciparum* apicortin with α-and β-tubulin is critical for parasite growth and survival. Sci. Rep. *11*, 1–16.
17. Pamula, M.C., Ti, S.C., and Kapoor, T.M. (2016). The structured core of human β tubulin confers isotype-specific polymerization properties. J. Cell Biol. *213*, 425–433.
18. Hirst, W.G., Biswas, A., Mahalingan, K.K., and Reber, S. (2020). Differences in intrinsic tubulin dynamic properties contribute to spindle length control in *Xenopus* species. Curr. Biol. *30*, 2184–2190.e5.
19. Chaaban, S., Jariwala, S., Hsu, C.T., Redemann, S., Kollman, J.M., Müller-Reichert, T., Sept, D., Bui, K.H., and Brouhard, G.J. (2018). The structure and dynamics of *C. elegans* tubulin reveals the mechanistic basis of microtubule growth. Dev. Cell *47*, 191, e8–204.e8.
20. Delves, C.J., Ridley, R.G., Goman, M., Holloway, S.P., Hyde, J.E., and Scaife, J.G. (1989). Cloning of a β-tubulin gene from *Plasmodium falciparum*. Mol. Microbiol. *3*, 1511–1519.
21. Holloway, S.P., Gerousis, M., Delves, C.J., Sims, P.F., Scaife, J.G., and Hyde, J.E. (1990). The tubulin genes of the human malaria parasite *Plasmodium falciparum*, their chromosomal location and sequence analysis of the α-tubulin II gene. Mol. Biochem. Parasitol. *43*, 257–270.
22. Holloway, S.P., Sims, P.F.G., Delves, C.J., Scaife, J.G., and Hyde, J.E. (1989). Isolation of α-tubulin genes from the human malaria parasite, *Plasmodium falciparum*: sequence analysis of α-tubulin. Mol. Microbiol. *3*, 1501–1510.
23. Rawlings, D.J., Fujioka, H., Fried, M., Keister, D.B., Aikawa, M., and Kaslow, D.C. (1992). α-Tubulin II is a male-specific protein in *Plasmodium falciparum*. Mol. Biochem. Parasitol. *56*, 239–250.
24. Fennell, B.J., Al-Shatr, Z.A., and Bell, A. (2008). Isotype expression, post-translational modification and stage-dependent production of tubulins in erythrocytic *Plasmodium falciparum*. Int. J. Parasitol. *38*, 527–539.
25. Schwanhäusser, B., Busse, D., Li, N., Dittmar, G., Schuchhardt, J., Wolf, J., Chen, W., and Selbach, M. (2011). Global quantification of mammalian gene expression control. Nature *473*, 337–342.
26. Roll-Mecak, A. (2019). How cells exploit tubulin diversity to build functional cellular microtubule mosaics. Curr. Opin. Cell Biol. *56*, 102–108.
27. Janke, C., and Magiera, M.M. (2020). The tubulin code and its role in controlling microtubule properties and functions. Nat. Rev. Mol. Cell Biol. *21*, 307–326.
28. Read, M., Sherwin, T., Holloway, S.P., Gull, K., and Hyde, J.E. (1993). Microtubular organization visualized by immunofluorescence microscopy during erythrocytic schizogony in *Plasmodium falciparum* and investigation of post-translational modifications of parasite tubulin. Parasitology *106*, 223–232.
29. Xu, Z., Schaedel, L., Portran, D., Aguilar, A., Gaillard, J., Marinkovich, M.P., Théry, M., and Nachury, M.V. (2017). Microtubules acquire resistance from mechanical breakage through intralumenal acetylation. Science *356*, 328–332.
30. Bieling, P., Kandels-Lewis, S., Telley, I.A., van Dijk, J., Janke, C., and Surrey, T. (2008). CLIP-170 tracks growing microtubule ends by dynamically recognizing composite EB1/tubulin-binding sites. J. Cell Biol. *183*, 1223–1233.
31. Peris, L., Wagenbach, M., Lafanechère, L., Brocard, J., Moore, A.T., Kozielski, F., Job, D., Wordeman, L., and Andrieux, A. (2009). Motor-dependent microtubule disassembly driven by tubulin tyrosination. J. Cell Biol. *185*, 1159–1166.
32. Nirschl, J.J., Magiera, M.M., Lazarus, J.E., Janke, C., and Holzbaur, E.L.F. (2016). α-Tubulin tyrosination and CLIP-170 phosphorylation regulate the initiation of dynein-driven transport in neurons. Cell Rep *14*, 2637–2652.
33. McKenney, R.J., Huynh, W., Vale, R.D., and Sirajuddin, M. (2016). Tyrosination of α-tubulin controls the initiation of processive dynein–dynactin motility. EMBO J *35*, 1175–1185.
34. Bertiaux, E., Balestra, A.C., Bournonville, L., Louvel, V., Maco, B., Soldati-Favre, D., Brochet, M., Guichard, P., and Hamel, V. (2021). Expansion microscopy provides new insights into the cytoskeleton of malaria parasites including the conservation of a conoid. PLoS Biol *19*, e3001020.
35. Lacroix, B., van Dijk, J., Gold, N.D., Guizetti, J., Aldrian-Herrada, G., Rogowski, K., Gerlich, D.W., and Janke, C. (2010). Tubulin polyglutamylation stimulates spastin-mediated microtubule severing. J. Cell Biol. *189*, 945–954.
36. Valenstein, M.L., and Roll-Mecak, A. (2016). Graded control of microtubule severing by tubulin glutamylation. Cell *164*, 911–921.
37. Bonnet, C., Boucher, D., Lazereg, S., Pedrotti, B., Islam, K., Denoulet, P., and Larcher, J.C. (2001). Differential binding regulation of microtubule-associated proteins MAP1A, MAP1B, and MAP2 by tubulin polyglutamylation. J. Biol. Chem. *276*, 12839–12848.
38. Bannister, L.H., Hopkins, J.M., Dluzewski, A.R., Margos, G., Williams, I.T., Blackman, M.J., et al. (2003). *Plasmodium falciparum* apical membrane antigen 1 (PfAMA-1) is translocated within micronemes along subpellicular microtubules during merozoite development. J. Cell Sci. *116*, 3825–3834.
39. Mitchison, T., and Kirschner, M. (1984). Dynamic instability of microtubule growth. Nature *312*, 237–242.
40. Wieczorek, M., Bechstedt, S., Chaaban, S., and Brouhard, G.J. (2015). Microtubule-associated proteins control the kinetics of microtubule nucleation. Nat. Cell Biol. *17*, 907–916.
41. Gómez-de-Mariscal, E., Guerrero, V., Sneider, A., Jayatilaka, H., Phillip, J.M., Wirtz, D., and Muñoz-Barrutia, A. (2021). Use of the p-values as a size-dependent function to address practical differences when analyzing large datasets. Sci. Rep. *11*, 20942.
42. Lyons-Abbott, S., Sackett, D.L., Wloga, D., Gaertig, J., Morgan, R.E., Werbovetz, K.A., and Morrissette, N.S. (2010). α-Tubulin mutations alter oryzalin affinity and microtubule assembly properties to confer dinitroaniline resistance. Eukaryot. Cell *9*, 1825–1834.
43. Morejohn, L.C., and Fosket, D.E. (1991). The biochemistry of compounds with anti-microtubule activity in plant cells. Pharmacol. Ther. *51*, 217–230.
44. Morgan, R.E., Ahn, S., Nzimiro, S., Fotie, J., Phelps, M.A., Cotrill, J., Yakovich, A.J., Sackett, D.L., Dalton, J.T., and Werbovetz, K.A. (2008). Inhibitors of tubulin assembly identified through screening a compound library. Chem. Biol. Drug Des. *72*, 513–524.
45. Morrissette, N. (2015). Targeting *Toxoplasma* tubules: tubulin, microtubules, and associated proteins in a human pathogen. Eukaryot. Cell *14*, 2–12.
46. Soleilhac, E., Brillet-Guéguen, L., Roussel, V., Prudent, R., Touquet, B., Dass, S., Aci-Sèche, S., Kasam, V., Barette, C., Imberty, A., et al. (2018). Specific targeting of plant and apicomplexa parasite tubulin through differential screening using in silico and assay-based approaches. Int. J. Mol. Sci. *19*, 3085.
47. Hirst, W.G., Kiefer, C., Abdosamadi, M.K., Schäffer, E., and Reber, S. (2020). *In vitro* reconstitution and imaging of microtubule dynamics by fluorescence and label-free microscopy. STAR Protoc *1*, 100177. https://doi.org/10.1016/j.xpro.2020.100177.
48. Schindelin, J., Arganda-Carreras, I., Frise, E., Kaynig, V., Longair, M., Pietzsch, T., Preibisch, S., Rueden, C., Saalfeld, S., Schmid, B., et al. (2012). Fiji: an open-source platform for biological-image analysis. Nat. Methods *9*, 676–682.
49. Allen, R.J.W., and Kirk, K. (2010). *Plasmodium falciparum* culture: the benefits of shaking. Mol. Biochem. Parasitol. *169*, 63–65.
50. Hyman, A.A., Salser, S., Drechsel, D.N., Unwin, N., and Mitchison, T.J. (1992). Role of GTP hydrolysis in microtubule dynamics: information

from a slowly hydrolyzable analogue. GMPCPP. Mol. Biol. Cell *3*, 1155–1167.

51. Kapoor, V., Hirst, W.G., Hentschel, C., Preibisch, S., and Reber, S. (2019). MTrack: automated detection, tracking, and analysis of dynamic microtubules. Sci. Rep. *9*, 3794.
52. Lambros, C., and Vanderberg, J.P. (1979). Synchronization of *Plasmodium falciparum* erythrocytic stages in culture. J. Parasitol. *65*, 418–420.
53. Shevchenko, A., Wilm, M., Vorm, O., and Mann, M. (1996). Mass spectrometric sequencing of proteins silver-stained polyacrylamide gels. Anal. Chem. *68*, 850–858.
54. Suckau, D., Resemann, A., Schuerenberg, M., Hufnagel, P., Franzen, J., and Holle, A. (2003). A novel MALDI LIFT-TOF/TOF mass spectrometer for proteomics. Anal. Bioanal. Chem. *376*, 952–965.
55. Rappsilber, J., Mann, M., and Ishihama, Y. (2007). Protocol for micro-purification, enrichment, pre-fractionation and storage of peptides for proteomics using StageTips. Nat. Protoc. *2*, 1896–1906.
56. Tyanova, S., Temu, T., and Cox, J. (2016). The MaxQuant computational platform for mass spectrometry-based shotgun proteomics. Nat. Protoc. *11*, 2301–2319.

STAR★METHODS

KEY RESOURCES TABLE

REAGENT or RESOURCE	SOURCE	IDENTIFIER
Antibodies		
Anti-Tubulin (clone DM1A)	Sigma-Aldrich	Cat #T9026; RRID: AB_477593
Anti-Rhodamine antibody (clone 11H10)	Thermo Fisher Scientific	Catalog # 200-301-246
Anti-Tubulin (clone B-5-1-2)	Sigma-Aldrich	Cat #: T5168; RRID: AB_477579
Anti-Detyrosinated alpha-Tubulin	Abcam	Cat #: ab48389; RRID: AB_869990
Anti-Tubulin antibody [YL1/2] (GEEEGEEY)	Abcam	Cat #: ab6160; RRID: AB_305328
Anti-Acetylated alpha-Tubulin (clone 6-11B-1)	Sigma-Aldrich	Cat #: T7451; RRID: AB_609894
Anti-Phosphoserine	Abcam	Cat #: ab9332; RRID: AB_307184
Anti-Polyglutamylation modification	AdipoGen Life Sciences	GT335
Anti-*Plasmodium falciparum* HSP70 (aa 365-681)	LifeSpan BioSciences	Cat #: LS-C109068-25
HRP-conjugated anti-rabbit IgG	Proteintech	Proteintech 0001-2
Anti-mouse IgG	Proteintech	Proteintech 0001-1
Chemicals, Peptides, and Recombinant Proteins		
Oryzalin	Sigma-Aldrich	Cat #: 36182
Amiprofos-Methyl (AMP)	Sigma-Aldrich	Cat #: 03992
Tubulin (*Xenopus*)	Hirst et al.[18]	N/A
Tubulin (*Plasmodium falciparum*)	This manuscript	N/A
Tubulin (HEK)	This manuscript	N/A
Tubulin (Bovine brain)	This manuscript	N/A
Tubulin (biotinylated)	Hirst et al.[47]	N/A
Anhydrous DMSO	Life Technologies	D12345
Piperazine-1,4-bis(2-ethanesulfonic acid) (PIPES)	Sigma-Aldrich	Cat #: P1851
Methylcellulose	Sigma-Aldrich	Cat #: 94378
NeutrAvidin Protein	Thermo-Fisher	Cat #: 31000
k-Casein from bovine milk	Sigma-Aldrich	Cat #: C0406
Chlorotrimethylsilane (TMCS)	Sigma-Aldrich	Cat #: 386529
GMPCPP	Jena Bioscience	Cat #: NU-405L
Pluronic F-127	Sigma-Aldrich	Cat #: P2443
Protocatechuic Acid (PCA)	Sigma-Aldrich	Cat #: 03930590
Protocatechuate-3,4-dioxygenase (PCD)	Sigma-Aldrich	Cat #: P8279
Trolox	Sigma-Aldrich	Cat #: 238813
Magnesium chloride hexahydrate ($MgCl_2 \cdot 6H_2O$)	Carl Roth	Cat #: HN03.2
Glycerol	Carl Roth	Cat #: 3783.4
DTT	Sigma-Aldrich	Cat #: 43815
β-Mercaptoethanol	Sigma-Aldrich	Cat #: M6250
Benzonase	Merck Millipore	Cat #: 70664
Ammonium sulfate ($(NH_4)_2SO_4$)	Carl Roth	Cat #: 3746.1
SYBR Safe	Sigma-Aldrich	Cat #: S7563
TRIS	Carl Roth	Cat #: 4855.5
Triton X-100	Carl Roth	Cat #: 3051.2
GTP	Sigma-Aldrich	Cat #: G8877
ATP	Sigma-Aldrich	Cat #: A26209
EGTA	Sigma-Aldrich	Cat #: E3889
EDTA	Carl Roth	Cat #: 8043.1

(*Continued on next page*)

Continued		
REAGENT or RESOURCE	SOURCE	IDENTIFIER
Chloroquine	Sigma-Aldrich	Cat #: C6628
PBS	PAN Biotech	Cat #: P04-361000
RPMI 1640	Gibco	Cat #: 51800043
Lglutamine	Gibco	Cat #: 25030081
HEPES	Merck Millipore	Cat #: H3375-500G
Glucose	Carl Roth	Cat #: X997.2
DMEM	ThermoFisher	Cat #: 11995073
Giemsa solution	VWR Chemicals	Cat #: 350864X
Gentamycin	Thermo-Fisher	Cat #: 15750060
Hypoxanthine	Sigma-Aldrich	Cat #: H-9636-25G
AlbuMAX II	Gibco	Cat #: 11021045
Fetal bovine serum	Thermo-Fisher	Cat #: 16000044
Sorbitol	Sigma-Aldrich	Cat #: S3889-500G
Saponin	Sigma-Aldrich	Cat #: S4521-10G
Formic acid (LC-MS grade)	Thermo Fisher Scientific	Cat #: 85178
Trifluoroacetic acid (TFA)	Carl Roth	Cat #: P088.1
Acetonitile (LC-MS grade)	VWR Chemicals	Cat #: 83640.400
Water (LC-MS grade)	Carl Roth	Cat #: AE72.2
Trypsin	Promega	Cat #: V5111
Urea	Sigma-Aldrich	Cat #: U5128-100G
Thiourea	Sigma-Aldrich	Cat #: T8656
Iodoacetamide	Sigma-Aldrich	Cat #: I1149
Ammonium bicarbonate	Sigma-Aldrich	Cat #: A6141
α-cyano-4-hydroxycinnamic acid (CHCA)	Sigma-Aldrich	Cat #: 476870
Other – Equipment		
Coverslides, 22×22 mm	Corning	Cat #: 2850-55
Coverslips, 18×18 mm	Thermo Scientific Menzel	Cat #: 15757572
Ultra-clear centrifuge tubes	Beckman Coulter	Cat #: 344057
PD-10 desalting columns	GE Healthcare	Cat #: 17085101
TOG-column	Reusch at al.[10] and Widlund et al.[11]	N/A
0.45-μm Milliex-HV polyvinylidene fluoride membrane	Millipore, Bedford, MA	SLHV033RB
Amicon Ultra 30K MWCO centrifugal filter	Millipore	UFC803024
Software & Algorithms		
GraphPad Prism v8.0.1	GraphPad	https://www.graphpad.com
R v4.1.1	R Foundation for Statistical Computing	https://www.r-project.org/
Fiji	Schindelin et al.[48]	https://imagej.net/software/fiji/

RESOURCE AVAILABILITY

Lead contact

Further information and requests for resources and reagents should be directed to and will be fulfilled by the lead contact, Simone Reber (simone.reber@iri-lifesciences.de).

Materials availability

Purified *P. falciparum* or HEK tubulin generated in this study will be made available on request, but we may require a payment and/or a completed Materials Transfer Agreement if there is potential for commercial application.

Data and code availabilty

- All data reported in this paper will be shared by the lead contact upon request.

- This paper does not report original code.
- Any additional information required to reanalyze the data reported in this paper is available from the lead contact upon request.

EXPERIMENTAL MODEL AND SUBJECT DETAILS

Chloroquine (CQ)-sensitive 3D7 wild-type strain of *P. falciparum*

The chloroquine (CQ)-sensitive 3D7 wild-type strain of *P. falciparum* was used for all cell culture and purification of *P. falciparum* tubulin. Parasites were cultured in complete culture RPMI-1640 medium (CCM) (supplemented with 3 mM L-glutamine, 25 mM HEPES, 20 mM glucose, 24 μg/mL gentamycin, 200 μM hypoxanthine, and 0.6 % AlbuMAX II bovine serum albumin). Routine cultures were maintained at 3–4% haematocrit in a 37°C incubator with a gas mixture of 1% CO_2, 3% O_2, and 96% N_2 on a shaking platform.[49] Parasitaemia was monitored every 24 - 48 hours by Giemsa stain and cultures were split when the parasitaemia reached 1 – 10 %.

HEK293 cell line

Human embryonic kidney (HEK) 293 cells (ATCC, CRL-1573) were grown in humidified incubator at 37°C in 5% CO_2 and 95% O_2. The cells were cultured in high-glucose DMEM containing 10% fetal bovine serum, and 50 μg/mL gentamicin. Cells were passaged every 3 – 4 days, at 1:5 or 1:10 dilutions.

METHOD DETAILS

Preparation of GMPCPP-stabilized microtubule seeds

To serve as nucleation templates for *in vitro* microtubule assembly, stabilized microtubule seeds were prepared using GMPCPP, a slowly-hydrolyzing GTP analogue that prevents rapid microtubule depolymerization[50]. Additionally, biotinylated tubulin was incorporated to facilitate adhesion to the surface of neutravidin-functionalized coverslips, and labelled tubulin was used to visualize the seeds. A seed assembly reaction was prepared on ice by mixing bovine brain tubulin (final concentration 2.8 μM), fluorescently labelled tubulin (final concentration 0.4 μM), biotin-labeled tubulin (final concentration 0.8 μM), $MgCl_2$ (final concentration 2 mM, and GMPCPP (final concentration 1 mM) in 1x BRB80 (80 mM PIPES, 1 mM $MgCl_2$ and 1 mM EGTA, pH 6.9) in a microreaction tube. The reaction was left on ice for 10 minutes to allow for nucleotide exchange, and then transferred to a ThermoMixer (Eppendorf) and incubated at 37°C for 2 hours. The reaction was then removed from the incubator and microtubules were gently resuspended by flicking the tube. Using a 200 μL pipette with cut-off tip to avoid shearing, the suspension was gently layered over 100 μL of a pre-warmed (37°C) 1x BRB80 solution supplemented with 60 % v/v glycerol and 0.5 mM GMPCPP in a 230 μL thick-walled centrifuge tube (Beckman-Coulter). Care was taken to maintain the two distinct liquid phases. The reaction was centrifuged in a pre-warmed (37°C) TLA-100 rotor at 220,000 x g for 10 minutes at 35°C. The top layer was removed, and the cushion interface was washed with warm 1x BRB80, after which the cushion was removed, and the pellet was gently washed twice with warm 1x BRB80. Finally, the pellet was resuspended in warm 1x BRB80 supplemented with 1 mM DTT using a cut-off pipette tip, separated into 5 μL working aliquots, flash-frozen in liquid nitrogen and stored at -80°C.

TIRF assays, image acquisition, and data processing

Flow chambers were constructed with glass coverslips passivated with trimethylchlorosilane as described in[47] and mounted onto passivated glass slides using thin strips of parafilm. Chambers were functionalized by perfusing 20 μL of 100 mg/mL Neutravidin in 1x BRB80 through the chamber, and incubating for 5 min at room temperature. The chamber was rinsed twice with 20 μL 1x BRB80, twice with a blocking buffer consisting of 1% w/v Pluronic F-127 in 1x BRB80, and incubated at room temperature for 15 min. Wash buffer containing 1 mg/mL K-casein in 1x BRB80 was flowed through the chamber followed by 2 x 20 μL of GMPCPP-stabilized microtubule seeds containing 10% Atto565- or Atto647-labeled and 20% biotin-labeled tubulin suspended in wash buffer.

Polymerization reactions were carried out at 37°C in 1x BRB80 buffer supplemented with 2 mM GTP, 1 mg/mL k-casein, 1% β-mercaptoethanol, 2 mM Trolox, 2.5 mM PCA, 25 nM PCD, and 0.15 % methylcellulose at different concentrations of purified tubulin with 10 % Atto565- or Atto488-labeled porcine brain tubulin. In the case of 6 μM tubulin reactions, glycerol was added to a final concentration of 10 % v/v to promote microtubule growth at low tubulin concentrations. 30 - 50 μL of reaction solution were perfused through the chamber, then both ends were sealed with silicone grease. The slide was mounted on the objective and left for 10 min to allow the temperature to equilibrate before imaging.

Images were taken on an inverted Nikon Eclipse Ti-E microscope with a motorized TIRF angle, a Nikon Plan Apochromat 100x/1.49NA oil immersion objective lens, and a Photometrics Prime 95B sCMOS camera. Atto488-labeled microtubules were imaged with a 488 nm laser, Atto565-labeled microtubules were imaged with a 561 nm laser and Atto647-labeled microtubule seeds were imaged with a 647 nm laser. Time-lapse images were taken at a frame rate of 0.2 fps with an exposure time of 100 - 200 ms. Recording was controlled with the Nikon ND Acquisition software.

Microtubule dynamics were measured by producing kymographs using the Multi Kymograph function of the FIJI image analysis software[48] and manually fitting lines to growth and shrinkage events according to.[47,51] Growth and shrinkage velocities were

calculated from the slopes of the fitted lines. Catastrophe frequencies were calculated as the inverse of the mean of microtubule lifetimes. Rescue frequencies were calculated as the inverse of the mean duration of depolymerization events; events without a rescue were assigned a value of 0.

Synchronization of *P. falciparum* cultures

P. falciparum cultures were synchronised using the sorbitol haemolysis technique.[52] Cultures with >1 % ring-stage parasitaemia were centrifuged at 500 x g for 5 minutes at room temperature and the supernatant was discarded. Pellets were resuspended in 10 pellet volumes of pre-warmed (37°C) 5 % w/v sorbitol and incubated at 37°C for 15 minutes. The cell suspension was centrifuged again for 5 minutes at 500 x g at room temperature, the supernatant was discarded, and the pellet was resuspended in CCM to the desired haematocrit to continue culturing the parasites.

Purification of *P. falciparum* tubulin

To purify tubulin from *Pf*, parasite cells were first isolated from host red blood cells by saponin lysis. Synchronized cultures at >5 % parasitaemia were pelleted at 500 x g at 4°C in a Beckmann 5810 R centrifuge and the supernatant was discarded. The pellet was resuspended on ice in an equal volume of saponin lysis buffer (1x PBS, 0.15 % w/v saponin) and incubated on ice for 5 minutes with occasional inversion of the tube. The pellet was centrifuged for 5 minutes at 500 x g at 4°C, the supernatant was discarded, and the pellet was resuspended in a volume of 1x PBS equivalent to the total original saponin lysis suspension. The pellet was again centrifuged and the 1x PBS wash was repeated twice. Finally, the pellet was resuspended in a minimal volume of 1x PBS (1 mL or less), flash frozen, and stored at -80°C. On the day of tubulin purification, aliquots were quickly thawed, pooled, resuspended in 1x BRB80, and supplemented with 100 μM GTP, 2 mM DTT, and 1x protease inhibitors. Cells were sonicated at full power at 0.5 second intervals totaling 30 seconds with a sonicator probe (Sonorex GM 2070) and then centrifuged for 10 minutes at 80,000 rpm (440,000 x g) at 4°C in an MLA-80 rotor. The supernatant was loaded at 0.5 CV/min onto a TOG-column preequilibrated with 1× BRB80. The flow rate was then changed to 1 CV/min for the following wash steps: 1) 10 CV of 1× BRB80, 100 μM GTP; 2) 3 CV of 1× BRB80, 100 μM GTP, 10 mM $MgCl_2$, 5 mM ATP followed by a 15-min incubation; 3) 5 CV of 1× BRB80 and 100 μM GTP. The tubulin was eluted with 3 CV of 1× BRB80, 100 μM GTP, and 500 mM $(NH_4)_2SO_4$. Pooled fractions were desalted into 1× BRB80 and 10 μM GTP with a PD10 desalting column and concentrated using an Amicon Ultra 30K MWCO centrifugal filter (Millipore). Tubulin was aliquoted and snap frozen in liquid nitrogen.

Purification of HEK tubulin

HEK293 cells were pelleted and resuspended in an equal volume of 1× BRB80 containing 3 U of benzonase, 1 mM DTT, and protease inhibitors. Cells were lysed by douncing on ice and the lysate was cleared by centrifugation at 80,000 rpm (440,000 x g) in a pre-cooled MLA-80 rotor at 2°C for 30 minutes and then filtered through a 0.45-μm Milliex-HV polyvinylidene fluoride membrane. The filtrate was loaded onto an equilibrated TOG-column. Tubulin was eluted, desalted, concentrated and flash-frozen in liquid nitrogen as described above.

Purification of bovine brain tubulin

Frozen bovine brain tissue stored at -80°C was pulverized using a mortar and pestle on dry ice, and then suspended in 1x BRB80 supplemented with benzonase, 1 mM DTT, protease inhibitors, and 10 μg/mL Cytochalasin D at a ratio of 1 mL buffer : 1 g brain tissue on ice. The tissue suspension was sonicated at full power at 0.5 second intervals totalling one minute with a sonicator probe (Sonorex GM 2070) and then further homogenized using 20 strokes with a cell douncer on ice. The lysate was centrifuged for 10 minutes at 80,000 rpm (440,000 x g) at 4°C in an MLA-80 rotor, the supernatant was loaded onto an equilibrated TOG-column, and the tubulin purification proceeded as described above.

Parasite proliferation assays

Synchronous blood-stage *P. falciparum* cultures between 1 % and 7 % parasitaemia were used for parasite proliferation dose-response assays. Uninfected red blood cells (uRBCs) were prepared by adding 2 mL of fresh uRBCs to 10 mL pre-warmed CCM and incubating at 37°C for up to 1 hour. A 10 mL aliquot of culture suspension was then removed from the culture flask and the iRBCs (infected red blood cells) were washed by centrifuging at 500 x g for five minutes, removing the supernatant, resuspending the pellet in 10 mL CCM, and incubating for 1 hour in a 37°C water bath while the parasitaemia was counted and the assay solutions were prepared. Tubes containing uRBCs and iRBCs were inverted every 15 – 20 min to keep the cells suspended. Medium containing the inhibitor of interest was prepared by diluting the inhibitor stock in CCM and filter-sterilising the solution through a 0.2 μm syringe filter. The working solution inhibitor concentration was 2x the highest concentration tested during the assay. The volume of CCM used corresponded to the number of rows of the 96-well culture plate used for each inhibitor. Generally, 1.6 mL of medium was prepared each time, corresponding to 200 μL per row for 3 technical replicates plus 1 mL extra in case any solution was lost during filtering. Additionally, CCM containing 1 mM chloroquine (CQ) was prepared as a positive control in the same manner to a final volume of 1 mL per plate. Dose-response assays were carried out in 96-well culture plates with the rows labelled A – H and the columns labelled 1 – 12. Only rows B – G and columns 2 – 11 contained samples; all peripheral wells contained 200 μL RPMI to prevent evaporation from experimentally important wells. To prepare the wells for cell culture, 100 μL of CQ working solution were added to the remaining wells of column 2, 200 μL of each inhibitor working solution were added to column 4, and 100 μL of CCM were added to the

remaining wells. The inhibitor solution of column 4 was then serially diluted at a ratio of 1:2 from column 4 to column 11, leaving a volume of 100 μL in each well. To prepare the working iRBC cell suspension, the iRBC and uRBC suspensions were removed from the water bath, centrifuged at RT for 5 min at 500 x g, and the supernatant was discarded. iRBCs and uRBCs were resuspended in CCM at an appropriate ratio to achieve 2 % hematocrit at 0.5 % parasitaemia. Aliquots (100 μL) of the cell suspension were added to each well to achieve a final culture volume of 200 μL at 1 % hematocrit. Finally, plates were incubated in sealed humidified chambers with 3 % oxygen and 1 % CO_2 (with the balance being N_2) and incubated at 37°C, without shaking, for 96 h. Parasite proliferation was quantified by measuring the quantity of DNA using the DNA dye SYBR Safe. At the end of 96 hours, cell cultures were resuspended in their wells, 100 μl were transferred to a new 96-well plate, and mixed with a lysis buffer (20 mM TRIS, 5 mM EDTA, 0.008 % w/v saponin, 0.08 % v/v Triton X-100, pH 7.5) containing 0.02 % v/v SYBR Safe dye. Fluorescence at 490 nm excitation and 520 nm emission wavelengths was measured using a FLUOstar OPTIMA plate reader (BMG Labtech). The signals were normalized to a scale of 0 – 100 % based on the mean signals of the CQ-treated (0 %, column 2) and untreated (100 %, column 3) wells. To determine IC_{50} values, the data were fit to a four- parameter logistic regression model using the GraphPad Prism.

Intact protein mass spectrometry

The purified *Pf* tubulin was analyzed using the Ultimate 3000 liquid chromatography system connected to a Q Exactive HF mass spectrometer via the ion max source with HESI-II probe (Thermo Scientific). The following MS source parameters were used: spray voltage 3.6 kV, capillary temperature 320°C, sheath gas 10, auxiliary gas 4, S-lens RF level 60, intact protein mode on. For the analysis 2 μL (approx. 1.3 μg of total protein) of the sample were desalted and concentrated by injection on a reversed-phase cartridge (MSPac DS-10, 2.1×10 mm, Thermo Scientific) at 60°C using buffer A (0.1 % formic acid, 5 % acetonitrile in water) at a constant flow rate of 22 μL/min for 3 min. This was followed by a short linear gradient of 5 % – 95 % buffer B (0.1 % formic acid in 80 % acetonitrile, 20 % water) within 10 min followed by washing and re-equilibration. Full MS spectra were acquired using the following parameters: mass range m/z 600–2500, resolution 15,000, AGC target $3x10^6$, μscans 5, maximum injection time 200 ms. MS raw data were analysed using BioPharma Finder (version 3.2, Thermo Scientific). First, an averaged spectrum over the chromatographic peak was generated followed by spectral deconvolution using a deconvolution mass tolerance of 5 ppm and a relative abundance threshold of 10 %.

Peptide mass fingerprint analysis by MALDI-MS

Purified *Pf* tubulin was separated by SDS-PAGE (Figure S2C), and bands of α- and ß-tubulin were excised separately and subjected to trypsin in-gel digestion as described previously.[53] Peptide masses were recorded by matrix-assisted laser desorption ionization-time of flight mass spectrometry (MALDI-TOF-MS) using an Ultraflex-II TOF/TOF instrument (Bruker Daltonics, Bremen, Germany) equipped with a 200 Hz solid-state Smart beam™ laser. We used α-cyano-4-hydroxycinnamic acid (CHCA) as the matrix and applied the protein digest samples using the dried droplet technique. The mass spectrometer was operated in the positive reflector mode in the m/z range of 600–4000. Database searches were performed using Mascot (Matrix Science Ltd., http://www.matrixscience.com), with mass tolerance typically set at 75 ppm and one missed cleavage allowed. MS/MS spectra of selected peptides were acquired using the LIFT mode[54].

In-solution digestion of *P. falciparum* tubulin and LC-MS/MS analysis

Purified *Pf* tubulin (approximately 4 μg) was mixed with 50 μl of denaturation buffer (6 M urea, 2 M thiourea, 10 mM HEPES, 2.5 mM DTT, pH 8.0) and incubated for 30 minutes. The reactions were then alkylated by adding 5 mM iodoacetamide (final concentration) and incubated for 20 minutes in the dark. In order to reduce the concentration of urea below 2 M, samples were diluted with four volumes of 50 mM ammonium bicarbonate (ABC) and digested overnight with 0.2 μg of sequencing-grade modified trypsin at 37°C. On the next day, the digestion was stopped by adding formic acid (FA) to a final concentration of 1 % and peptides were desalted using the Stage-tip protocol as described previously.[55] Finally, peptides were vacuum-dried and reconstituted in 10 μl of 0.05% TFA, 2% acetonitrile, and 6 μl were analyzed by a Ultimate 3000 reversed-phase capillary nano liquid chromatography system connected to a Q Exactive HF mass spectrometer (Thermo Fisher Scientific). Samples were injected and concentrated on a trap column (PepMap100 C18, 3 μm, 100 Å, 75 μm i.d. x 2 cm, Thermo Fisher Scientific) equilibrated with 0.05% TFA in water. After switching the trap column inline, LC separations were performed on a capillary column (Acclaim PepMap100 C18, 2 μm, 100 Å, 75 μm i.d. x 25 cm, Thermo Fisher Scientific) at an eluent flow rate of 300 nl/min. Mobile phase A contained 0.1 % formic acid in water, while mobile phase B contained 0.1 % formic acid in 80 % acetonitrile / 20 % water. The column was pre-equilibrated with 5 % mobile phase B followed by an increase of 5–44 % mobile phase B over 40 min. Mass spectra were acquired in a data-dependent mode utilising a single MS survey scan (m/z 350–1650) with a resolution of 60,000 in the Orbitrap, and MS/MS scans of the 15 most intense precursor ions with a resolution of 15,000. The dynamic exclusion time was set to 20 seconds and automatic gain control was set to $3x10^6$ and $1x10^5$ for MS and MS/MS scans, respectively.

MS and MS/MS raw data were analyzed using the MaxQuant software package (version 2.0.2.0) with implemented Andromeda peptide search engine[56] using the default parameters. In order to check for potential contaminations data were searched against the combined Uniprot reference proteome sequences of *Pf* (5,387 proteins, taxonomy 36329, last modified March 8, 2021), *Homo sapiens* (78,120 proteins, taxonomy 9606, last modified March 7, 2021) and Escherichia coli (5,062 proteins, taxonomy 83334, last modified March 7, 2021). For rough estimation of relative protein abundance, the iBAQ value is reported in the MaxQuant protein output table (Table S1)[25].

QUANTIFICATION AND STATISTICAL ANALYSIS

In each figure legend, details about the quantifications have been provided, including the number of events measured (n), the mean/median values, the SD/SEM. In addition, information about the statistical tests used for measuring significance and interpretation of p values is provided. P values greater than 0.05 are represented by "ns". A single * indicates a p value $\leq$ 0.05, ** indicates p values $\leq$ 0.01, *** indicates p values $\leq$ 0.001, and **** indicates p values $\leq$ 0.0001. For statistical analysis and plotting in this paper, we utilized Graphpad Prism version 8.0 for Mac OS X, GraphPad Software, La Jolla California USA, https://www.graphpad.com. When necessary, graph visuals such as line thickness, fonts, and colours were optimised using Adobe Illustrator.